SIN-CHN
SCIENTIFIC PRESS PTE.LTD.

Molecular & Cellular Biomechanics 2025, 22(1), 690.
https://doi.org/10.62617/mcb690

Article

Multi-frequency and multi-system GNSS positioning error modeling and correction based on machine learning in biomechanical context

Qi Liu, Jian Zhao*, Yuran Chen, Jiangshun Yu, Shan Wu, Sirui Wu

China Power Construction Group Guizhou Electric Power Design and Research Institute Co., LTD, Guizhou 550081, China
*** Corresponding author:** Jian Zhao, 18096171009@163.com

CITATION

Liu Q, Zhao J, Chen Y, et al. Multi-frequency and multi-system GNSS positioning error modeling and correction based on machine learning in biomechanical context. Molecular & Cellular Biomechanics. 2025; 22(1): 690. https://doi.org/10.62617/mcb690

ARTICLE INFO

Received: 1 November 2024
Accepted: 11 November 2024
Available online: 2 January 2025

Abstract: Positioning error modeling and correction in multi-frequency and multi-system GNSS is vital. Conventional methods have limitations in complex scenarios. Here, the RBF neural network algorithm is harnessed. GNSS and dual frequency data are integrated via multi-source feature extraction. K-means determines the RBF center to capture data traits. OLS optimizes the model. Through learning from extensive raw data, real-time error prediction and correction occur, resolving accuracy-complexity issues. In biomechanics, GNSS has great potential. In rehabilitation, it can precisely locate patients during outdoor mobility exercises. For example, for those recovering from orthopedic surgeries, GNSS tracks movement paths. This data correlates with biomechanical parameters like joint angles and muscle forces during walking or running. Understanding how patients' biomechanics change in different outdoor terrains and distances helps design personalized rehab plans. In sports, it monitors athletes' outdoor training. Analyzing position data alongside biomechanical metrics like sprint acceleration and body rotation during maneuvers refines training techniques. Experimentally, compared to RF, LSTM, and SVM, the RBF neural network's MSE dropped by 20.1%, 30.3%, and 44.4% respectively. Execution time reduced by 37.5%, 84.1%, and 64.7%. This enhanced GNSS method thus offers new prospects for biomechanical research and applications.

Keywords: positioning error modeling; positioning error correction; global navigation satellite system; machine learning algorithms; radial basis function neural network; biomechanics

1. Introduction

GNSS is the core of modern positioning technology and has a wide range of applications in transportation, surveying, agriculture, disaster monitoring, and other fields [1,2]. As the demand for GNSS applications continues to increase, higher requirements have also been put forward for its positioning accuracy. Traditional error modeling and correction methods often rely on physical models or empirical formulas, lack adaptability, are susceptible to satellite signal interference, and are difficult to effectively cope with complex and changing application environments. How to effectively model and correct the positioning errors of multi-frequency and multi-system GNSS is an important issue that urgently needs to be addressed in the field of navigation and positioning. With the increasing maturity of computer science, ML (Machine Learning) algorithms have made significant progress. ML algorithms can efficiently extract features from massive amounts of data and construct complex error models [3]. The use of ML algorithms for training and optimization, comprehensive analysis of different error sources, and real-time and efficient improvement of positioning accuracy can provide new ideas and methods for high-precision positioning problems in complex environments, which has important value and significance for promoting the development of intelligent positioning technology.

In order to improve the accuracy of multi-frequency and multi-system GNSS positioning and enhance the quality and level of system services, this article combines RBF neural network ML algorithm to study the modeling and correction of multi-frequency and multi-system GNSS positioning errors. Using a certain region as a sampling point, three GNSS observation stations are set up within the city, mountainous areas, and forests at the sampling point. Experimental analysis is conducted from four aspects: modeling accuracy, improvement after calibration, stability, and computational efficiency. In the analysis of modeling accuracy, the mean MSE of the model in this article decreases by 20.1%, 30.3%, and 44.4% compared to RF, LSTM, and SVM algorithms, respectively; in the analysis of the degree of improvement after correction, the model in this article is 6.9%, 9.6%, and 12.9% higher than the other three types of models, respectively; in stability analysis, compared with RF, LSTM, and SVM algorithms, the mean coefficient of variation (CV) of the calibration data in this article's model decreases by approximately 8.2%, 16.7%, and 21.1%, respectively; the average execution time of the algorithm in this article is 37.5%, 84.1%, and 64.7% less than the other three types of models, respectively. In practical applications, RBF neural networks can help improve the accuracy of error modeling and achieve real-time error correction.

2. Related works

Modeling and correcting GNSS positioning errors can significantly improve the quality of positioning services [4,5]. In order to improve the navigation capability of the positioning system, Shen et al. [6] proposed a hybrid navigation strategy of self-learning square root volume Kalman filter, which improved the optimal estimation accuracy through error compensation. The results indicated that the proposed method had long-term stability and could effectively improve the error correction effect [6]. Farrell et al. [7] achieved positioning error modeling and correction through sensor fusion state estimation, and integrated data from the Inertial Measurement Unit (IMU) using kinematic models. The results indicated that the proposed method had sufficient bandwidth accuracy, could reliably estimate the positioning state, and effectively achieved error modeling and correction [7]. To improve the positioning accuracy of GNSS, Abosekeen et al. [8] utilized fast orthogonal search for nonlinear error modeling, further improving the designed system to reduce excessive error growth and frequent GNSS interruptions. The results of road test trajectory evaluation showed that compared with existing technologies, the proposed method achieved significant performance improvement in positioning accuracy [8]. Morales et al. [9] developed a tightly coupled inertial navigation system assisted by environmental opportunity signals, using a radio synchronous positioning and mapping framework based on extended Kalman filters to correct positioning errors. The results indicated that the proposed method effectively improved the final position accuracy of the system [9]. The current research provides a certain reference for fine modeling and correction of error sources, but with the development of application environments, the complexity and nonlinear characteristics of error sources continue to increase. The current research methods lack stability and security, making it difficult to comprehensively consider all error sources.

The development of ML algorithms provides more possibilities for enhancing the stability and safety of GNSS [10,11]. Li et al. [12] proposed a positioning error evolution sharing framework based on deep neural networks, which achieved cooperation by sharing the positioning error evolution at specific times and locations. Extensive simulations based on actual data showed that the proposed framework had accuracy and security in positioning error correction and data sharing [12]. Fang et al. [13] used the LSTM algorithm to generate pseudo GNSS position increments that replace GNSS signals, achieving GNSS positioning error modeling by constructing the relationship between current and past information. The test results showed that compared with existing algorithms, the LSTM algorithm could improve the acquisition of more stable and reliable navigation and positioning solutions [13]. Ramavath et al. [14] proposed a new method for estimating positioning errors using ML techniques, which learned the relationship between position errors and the data added by GNSS receivers without any prior experience, and applied LSTM networks to model the temporal correlation of position error measurements. The results indicated that the proposed method could improve localization safety by training and learning position errors [14]. ML algorithms can effectively handle nonlinear relationships and complex input-output mappings, but typically require a large number of computational resources and are still limited in terms of real-time modeling accuracy.

3. Multi-frequency and multi-system GNSS positioning error modeling and correction

3.1. Multi-frequency and multi-system GNSS

3.1.1. GNSS signal structure

Multi-frequency and multi-system GNSS are an important component of modern navigation systems, providing high-precision positioning, velocity, and time information for global users. The structure of GNSS signals is crucial for ensuring navigation and positioning accuracy. It not only determines the transmission mode of the signal, but also directly affects the acquisition, tracking, decoding and other functions of the receiver [15,16]. The basic components of GNSS signals include carriers, spreading codes, and navigation data, as shown in **Figure 1**:

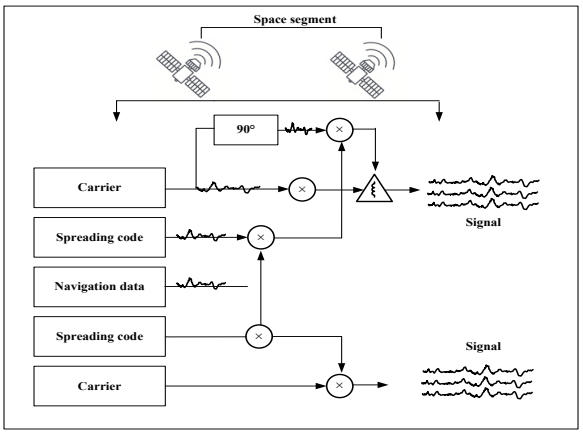

Figure 1. Basic composition of GNSS signals.

(1) Carrier wave

Carrier wave is a high-frequency sine wave used to carry spreading codes and navigation data. As the fundamental waveform of a signal, its frequency generally varies depending on the type of signal. At present, GNSS uses multiple frequency bands for signal transmission, and these frequency bands and corresponding carrier frequencies are also different. Taking GPS (Global Positioning System) and BeiDou as examples, as shown in **Table 1**, by using different frequency carriers, dual band or multi-band positioning can be achieved, effectively reducing errors caused by interference factors.

Table 1. Frequency bands and carrier frequencies used by GNSS systems.

System classification	The frequency band used	Carrier frequency	The services provided
GPS	L1	1575.42 MHz	Standard positioning service
	L2	1227.60 MHz	Military positioning service
	L5	1176.45 MHz	Civilian services
BeiDou	B1I	1561.098 MHz	Open service
	B2I	1207.14 MHz	Open service
	B3I	1268.52 MHz	Open service

(2) Spread spectrum code

Spread spectrum code is a pseudo-random sequence that can distinguish different satellite signals and perform rough ranging. It can be divided into two categories: Pseudo-Random Noise (PRN) code and Direct Sequence Spread Spectrum (DSSS) code. PRN code is used to achieve resolution of satellite signals, while DSSS is mainly used to enhance signal noise resistance. Each satellite has a unique spreading code, and the receiver identifies and captures the specific satellite signal based on the code.

(3) Navigation data

Navigation data is generally transmitted using carrier modulation, which carries important information such as satellite position and time. Each satellite regularly sends observation information and provides the orbit status and time stamp at a certain moment, so that the receiver can determine its relative position with the satellite. This data structure is generally organized in a certain format, which facilitates the receiving end to quickly extract and process the required information. After the receiver demodulates the received signal and analyzes the navigation data, accurate three-dimensional position information can be obtained.

3.1.2. GNSS receiver and signal processing

The core of GNSS positioning technology is to calculate the distance between the receiver and each satellite by calculating the time difference of the signals transmitted by each satellite [17]. Due to the known satellite position, the positioning information of the receiver on the Earth's surface can be obtained by using triangulation method. To achieve higher precision positioning, at least 4 satellites' signals need to be obtained, of which 3 satellites are used to measure longitude, latitude, and altitude information, and the remaining one is used to synchronize the clock bias of the receiver. According to different usage and accuracy requirements, GNSS receivers can be divided into consumer grade, professional grade, Real-time kinematic (RTK), and multi-system

multi-frequency receivers:

(1) Consumer grade receiver

Consumer grade receivers are terminals aimed at general users and have been widely used in daily navigation, mobile phone positioning, and portable electronic products. This type of receiver often uses C/A (Coarse Acquisition) encoding, with a positioning accuracy of only 3–5 m. Although the cost is low, its accuracy and performance are limited. Along with technological advancements, some consumer grade receivers have also begun to support the use of other systems, which has to some extent improved the compatibility of satellites and enhanced their positioning capabilities. Its universal usage environment includes car navigation, outdoor sports, tourism, geographical indications, etc.

(2) Professional grade receiver

As a high-precision and high-performance receiver, professional grade receivers have been widely used in land surveying, engineering construction, agricultural production, and other fields. This type of receiver generally supports the combination of multi-frequency technology, with an accuracy of up to 2 cm to 10 cm. Professional grade receivers generally have good anti-interference performance and can adapt well to the requirements of high-level surveying and positioning under complex working conditions. Its user group is mostly professional engineering and technical personnel, surveyors, and researchers who have a great demand for stable and accurate positioning data provided by the equipment.

(3) RTK receiver

RTK receiver is a high-precision device that can work in conjunction with mobile stations. Due to the use of differential processing technology and wireless real-time communication technology, it has been well applied in agriculture, civil engineering, unmanned driving and other fields. RTK receivers need to continuously receive reference station data to correct their positioning, which has great requirements for the working environment and requires operation in open areas. RTK receivers have become an indispensable and important means in modern surveying and automation operations due to their high precision, real-time performance, and other advantages.

(4) Multi-system multi-frequency receiver

A multi-system multi-frequency receiver can simultaneously receive signals from multiple GNSS systems in multiple bands, achieving joint positioning of multiple bands. This type of receiver has significant advantages in anti-interference performance and positioning accuracy, with measurement accuracy reaching sub meters or above. In areas with complex urban environments and high signal interference such as forests, multi-system multi-frequency receivers have better performance and are suitable for precision measurement, scientific research, and other fields. They are also suitable for professional users who require high reliability and have a wide range of applications.

In order to ensure the correct acquisition, tracking, and decoding of satellite signals by the receiver, signal processing is an important step, as shown in **Figure 2**:

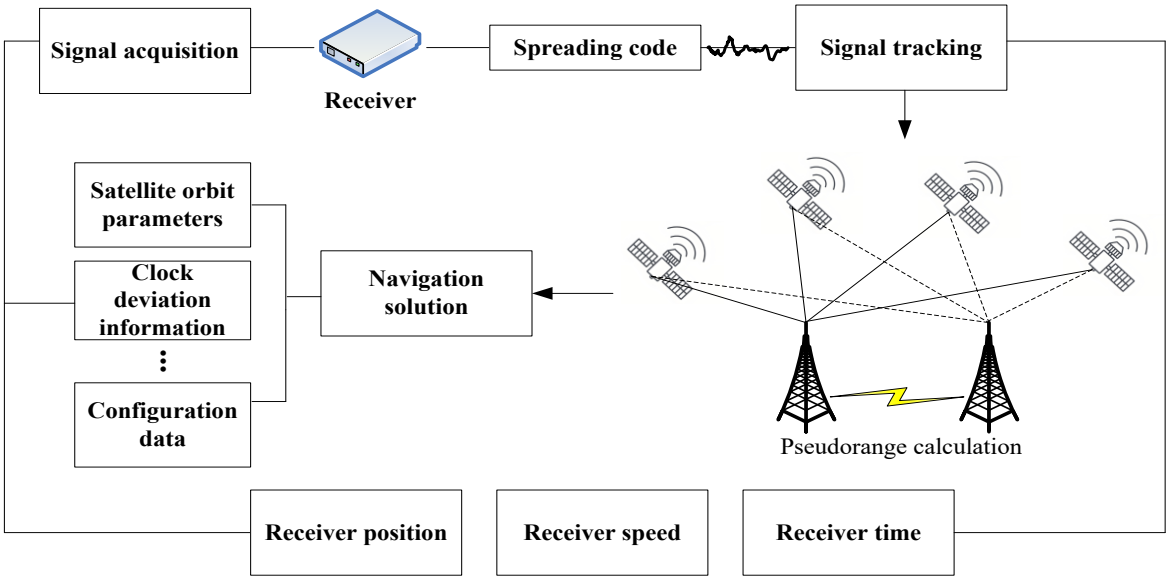

Figure 2. Receiver signal processing.

In **Figure 2**, the receiver receives signals from the satellite through an antenna, and signal acquisition is achieved by matching a specific spreading code to identify the satellite signal. The receiver uses known extension codes to search and capture satellite signals. In order to keep it synchronized with satellite signals, the receiver must perform continuous phase and frequency tracking on it. A closed-loop control method is used to dynamically adjust the locally replicated spreading code to match the received signal. Pseudo range is calculated based on the time of arrival of the measured signal. It refers to the straight-line distance between the receiver and the satellite plus errors caused by factors such as satellite clock bias, ionospheric and tropospheric delays. The receiver decodes satellite signals to obtain navigation data containing satellite orbit parameters and clock errors. By utilizing observed signals and combining them with pseudo range information, the receiver can determine its position, velocity, and time using methods such as triangulation and least squares estimation.

3.1.3. GNSS positioning error

GNSS positioning is based on precision timing and triangulation, and GNSS receivers use multiple satellite data to extract position information after calculation. During the transmission process, various factors can cause certain errors in the received signal, thereby reducing the accuracy of positioning. According to the sources and characteristics of GNSS errors, they can be divided into satellite errors, ionospheric errors, tropospheric errors, multipath effects, receiver errors, and user environment errors.

(1) Satellite error

In GNSS positioning error, satellite error is a significant factor that cannot be ignored, mainly including satellite orbit error and satellite clock error. The orbit error of a satellite is caused by the non-uniformity of the Earth's gravity field and gravitational disturbances from other celestial bodies. It is the deviation between the actual position of the satellite and the predicted position. This error makes the distance between the satellite and the receiver obtained by the receiver inaccurate. The satellite

clock bias is due to the fact that although the atomic clock installed on the satellite has high accuracy, there is still a small-time deviation. GNSS positioning is based on precision timing, and its errors have an impact on the calculation of signal transmission time, thereby adversely affecting positioning accuracy. Although satellite clocks are calibrated by ground-based control systems, even small-time errors can cause significant position errors.

(2) Ionospheric error

Ionospheric error refers to the interference caused by factors such as free electrons and high-energy particles when passing through the Earth's ionosphere, resulting in a change in signal transmission rate. The relevant data and characteristics are shown in **Table 2**:

Table 2. Ionospheric error related data and characteristics.

Sequence	Describe	Data or scope
1	Ionospheric altitude	60 km–1000 km
2	Free electron density	$10^{11} - 10^{12}$ electrons per cubic meter
3	Solar activity cycle	11 years
4	Signal frequency	High frequency has a relatively small impact, while low frequency has a significant impact.
5	Daytime error	The typical error is about 5 m–15 m.
6	Night time error	The typical error is about 2 m–15 m.

According to **Table 2**, at an altitude of 60 km–1000 km above the ground, the ionosphere is affected by solar radiation, and its internal atoms and molecules ionize to generate charged particles, resulting in delay or refraction of GNSS signals. The impact of ionospheric errors on signal transmission rate is determined by frequency, with high-frequency signals being less affected and low-frequency signals experiencing greater interference. This error is more pronounced during daytime, especially during periods of active solar activity, which can significantly reduce the positioning accuracy of GNSS.

(3) Tropospheric error

Tropospheric error refers to the error caused by the slow transmission rate of a satellite during its passage through the troposphere due to factors such as water vapor, air pressure, and temperature. The relevant data and characteristics are shown in **Table 3**:

Table 3. Tropospheric error related data and characteristics.

Sequence	Describe	Data or scope
1	Tropospheric altitude	0 km–12 km
2	Tropospheric water vapor	Typical range is 0 g/m^3–30 g/m^3.
3	Signal delay impact	Delay can reach 2–20 nanoseconds.
4	Changes in tropospheric thickness	The diurnal cycle changes by about 5%–15%.
5	Delay periodic variation	The daytime delay is about 10 m–20 m.

According to **Table 3**, the troposphere is an important region for climate change from the surface to an altitude of 12 km. The time delay effect of the troposphere on

spacecraft is directly related to its thickness, density, and other factors, and is influenced by water vapor, exhibiting diurnal cycle characteristics.

(4) Multipath effect

Multipath effect is the most common and complex error source in GNSS positioning. Due to the reflection and refraction of signals by objects such as buildings, ground, and trees, the receiver receives a superposition of direct and reflected waves. The reflection path is longer than the straight path. Therefore, this effect causes the receiver to obtain a larger pseudo range deviation, resulting in positioning errors. In complex terrain conditions such as cities, forests, and mountains, multipath effects are more prominent. Although the use of antenna structures, signal processing, and other methods can effectively suppress the above-mentioned effects, multipath effects remain an important factor restricting GNSS positioning accuracy in harsh environments.

(5) Receiver error

Receiver error refers to errors caused by various software and hardware components within the receiver, including clock errors, antenna errors, and signal processing errors. The relevant data and characteristics are shown in **Table 4**.

Table 4. Receiver error related data and characteristics.

Sequence	Describe	Data or scope
1	Clock error	The error is about 10^{-9} s–10^{-8} s.
2	Antenna phase center offset	Typical offset is about 1 mm–5 mm.
3	Differences in antenna azimuth performance	The positioning accuracy decreases by about 1 m–10 m.
4	Signal processing error	The signal processing error can reach 0.1 m–1 m.
5	Signal reception quality	The typical range of signal-to-noise ratio is 30 dB–50 dB.
6	Receiver sensitivity	The sensitivity is usually −130 dBm–150 dBm.

In **Table 4**, although the clock bias at the receiving end has been accurately calibrated, there is still a significant error compared to satellite atomic clocks, which leads to a decrease in timing accuracy and subsequently affects positioning accuracy. Antenna error refers to the deviation between the phase center of the receiving antenna and the actual center, or the difference in signal characteristics received by the antenna at different orientations. When processing satellite signals at the receiving end, additional errors may occur due to factors such as algorithms and computational accuracy. If the receiving quality of the receiver is poor or the sensitivity of the receiver is insufficient, it may lead to a decrease in the final positioning accuracy.

(6) User environment error

User environment error refers to the impact of factors such as the geographical and physical environment in which the receiving end is located on the positioning accuracy of the system in practical applications. In urban areas, the presence of high-rise buildings can interfere with satellite signals, leading to signal attenuation or loss, thereby reducing the accuracy of positioning; in mountainous or forested areas, undulating terrain and vegetation can also have a similar effect on signals. In addition, due to electromagnetic interference such as power lines and wireless devices around the receiver, it can also interfere with the satellite signals received by the receiver,

resulting in an increase in signal noise and a decrease in the stability of the positioning results.

3.2. ML algorithm

Traditional GNSS error correction methods rely on physical modeling and statistical analysis. Although they can reduce errors to a certain extent, their adaptive and generalization abilities are limited, especially in complex scenarios where their applications are restricted. ML algorithms can automatically extract features from massive historical data, construct models, and use new data to make predictions, making them highly valuable in error correction [18]. ML algorithm is a branch of artificial intelligence, and its "machine" refers to a computer. Unlike using program commands to execute assigned tasks, ML is built on the basis of big data. Its purpose is to "train" machines to "learn" knowledge from data, mine their inherent relationships, and use the "learned" knowledge to process new data and make corresponding judgments and predictions.

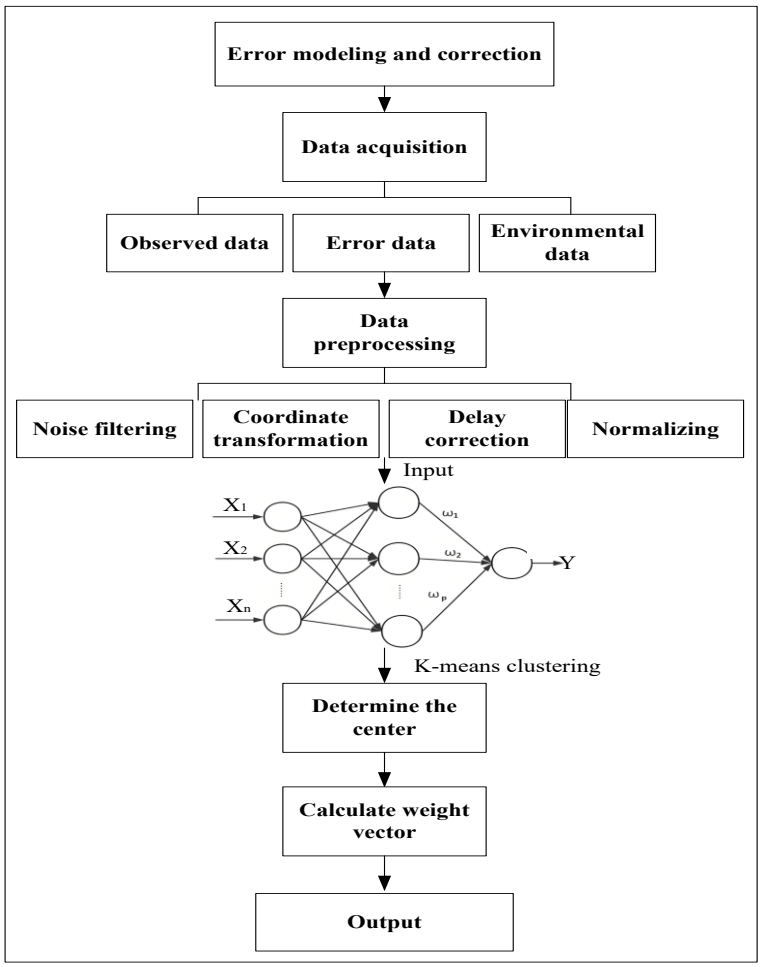

Figure 3. Error modeling and correction of RBF neural network.

RBF neural network is a feedforward neural network with strong nonlinear mapping ability. It uses RBF function as the excitation function to perform nonlinear transformation on training samples, achieving high-dimensional mapping of training samples [19]. This feature gives RBF networks significant advantages in handling

complex data relationships, especially in modeling and correcting GNSS positioning errors. By inputting data from multiple GNSS frequencies and systems into the RBF network, the RBF kernel function can capture complex errors caused by multipath effects, troposphere, ionosphere, and other factors during signal propagation. This article combines RBF neural network to model and correct the positioning error of multi-frequency and multi-system GNSS. The process is shown in **Figure 3**.

Firstly, GNSS observation data is collected and fixed stations are established in cities, mountains, forests, and other areas. The TrimbleR10 high-precision GNSS receiver is used for observation to obtain observation information, with a sampling rate set to 1Hz. Meanwhile, the height h_a of the antenna and the deviation Δh_a of the phase center are recorded. The VelodyneHDL-32E laser scanner is used to collect 3D environmental information such as weather data and geographic location data. The dual frequency joint observation data is used to invert ionospheric delay I_{if} and tropospheric delay T_{if}. For ionospheric delay:

$$I_{if} = \frac{f_1^2 f_2^2}{f_2^2 - f_1^2}\left(\frac{P_{i1} - P_{i2}}{f_1^2 f_2^2}\right) \tag{1}$$

f_1 and f_2 represent dual frequency carriers, and P_{i1} and P_{i2} are pseudo range observations at corresponding frequencies.

The Saastamoinen model is used to calculate tropospheric delay:

$$T_{if} = \frac{0.002277p}{z}\left(1 + 0.0026cos(2\phi) + \frac{0.00028h}{T}\right) \tag{2}$$

Among them, the parameter definitions of Formula 2 are shown in **Table 5**:

Table 5. Definition of parameters in Equation (2).

Sequence	Variables	Meaning
1	p	Pressure
2	z	Satellite zenith angle
3	ϕ	Site latitude
4	h	Altitude
5	T	Temperature

After obtaining the data, comprehensive preprocessing is performed on the data. The GNSS observation data is smoothed using Kalman filter to remove noise and outliers. The state formula and observation formula of the Kalman filter are [20]:

$$x_{k+1} = Ax_k + w_k \tag{3}$$

$$y_k = Hx_k + v_k \tag{4}$$

The variable definitions are shown in **Table 6**:

Table 6. Variable definitions for Equations (3) and (4).

Sequence	Variables	Meaning
1	x_k	State vector
2	A	State transition matrix
3	y_k	Observation vector
4	H	Observation matrix
5	w_k	Process noise
6	v_k	Observation noise

The observation data from different GNSS systems are uniformly converted into the World Geodetic System 84 coordinate system:

$$X = (N + h)cos\phi cos\lambda \tag{5}$$

$$Y = (N + h)cos\phi sin\lambda \tag{6}$$

$$Z = [(1 - e^2)N + h]sin\phi \tag{7}$$

Based on the collected 3D environmental data, the ray tracing algorithm is used to identify and eliminate abnormal observation values caused by multipath interference. For each observation data, its possible reflection path is calculated and compared with the direct path to eliminate false range errors that exceed the critical value.

According to Equations (1) and (2), I_{if} and T_{if} are calculated. The pseudo range observation data P_{if} is corrected, and the corrected pseudo range $P_{if}^{'}$ is obtained:

$$P_{if}^{'} = P_{if} - I_{if} - T_{if} \tag{8}$$

The preprocessed data as input is normalized to the RBF network:

$$X_{norm} = \frac{X - \mu x}{\sigma x} \tag{9}$$

In the RBF neural network algorithm, $X_1, X_2, \cdots, X_n$ represent the input sample data, and the output layer is the predicted error correction values $Y_1, Y_2, \cdots, Y_n$. The hidden layer of the RBF neural network is composed of several radial basis functions, and its output is represented as:

$$Y = \sum_{i=1}^{m} w_i \cdot \Phi_i(\|X - c_i\|) \tag{10}$$

Among them, m is the number of hidden neurons; w_i is the weight of the i-th neuron; c_i is the center of the i-th neuron; $\Phi_i(\cdot)$ is the RBF function:

$$\Phi_i(\|X - c_i\|) = exp\left(-\frac{\|X - c_i\|^2}{2\sigma_i^2}\right) \tag{11}$$

In the training of RBF neural network, the K-means clustering algorithm is used to determine the center c_i of RBF neural network:

$$c_i = \frac{1}{|S_i|}\sum_{x \in S_i} X \tag{12}$$

Among them, S_i is the sample set of the i-th cluster.

Using OLS for optimization, the weight vector is calculated:

$$W = (\Phi^t \Phi)^{-1} \Phi^t \hat{Y} \tag{13}$$

Among them, $\hat{Y}$ is the target error vector.

4. Positioning error modeling and calibration experiment

To verify the modeling and correction effect of multi-frequency and multi-system GNSS positioning error based on RBF neural network algorithm, this article conducts experimental analysis and compares it with widely used RF, LSTM, and SVM algorithms from four aspects: modeling accuracy, improvement degree after correction, stability, and computational efficiency.

4.1. Experimental data

This article takes a certain region as a sampling point, and sets up three GNSS observation stations in the city, mountainous areas, and forests of the sampling point. In order to expand the dataset and improve the generalization ability of the model under different environmental conditions, this paper adds GNSS observation stations in six specific scenarios: urban canyons, indoor environments, tunnel entrances and open water areas, farmland, and railway lines. Firstly, representative locations include densely populated city centers with high-rise buildings, interiors of different types of buildings, tunnel entrances, and near lakes. At each observation station, GNSS receivers, data loggers, weather stations, and environmental sensors will be deployed to comprehensively record GNSS raw data and meteorological data (temperature, humidity). Finally, a total of 9 regional scenes were collected using Trimble R10 high-precision GNSS receivers, and 3D environmental information around each observation site was recorded through laser scanning. Through long-term continuous observation, more than 500 hours of GNSS observation data were obtained. After inverting ionospheric and tropospheric delays, the collected data was preprocessed, and some basic information of the data was obtained as shown in **Table 7**:

Table 7. Basic information of some data.

Station number	Geographic location	Observation date	Antenna height (m)	Phase center deviation (m)	Ionospheric delay (m)	Tropospheric delay (m)	Temperature (℃)	Humidity (%)
1	City	2023-08-16	1.36	3.08	0.12	0.08	22.2	26
2	Mountainous region	2023-08-16	1.37	2.81	0.11	0.11	24.2	21
3	Forest	2023-08-16	1.41	2.95	0.11	0.10	22.5	52
4	Urban canyon	2023-08-16	1.41	3.07	0.14	0.12	19.8	23
5	Indoor environment	2023-08-16	1.25	2.98	0.10	0.10	25.3	19

Table 7. (*Continued*).

Station number	Geographic location	Observation date	Antenna height (m)	Phase center deviation (m)	Ionospheric delay (m)	Tropospheric delay (m)	Temperature (℃)	Humidity (%)
6	Tunnel entrance	2023-08-16	1.48	2.93	0.12	0.09	30.4	46
7	Open water	2023-08-16	1.41	3.15	0.12	0.10	28.8	28
8	Farmland	2023-08-16	1.21	3.18	0.12	0.07	31.2	23
9	Along the railway line	2023-08-16	1.25	2.93	0.11	0.11	25.2	42

The collected GNSS data is divided into training set, validation set, and test set in chronological order, with proportions of 70%, 15%, and 15%, respectively.

4.2. Experimental parameters

The parameter settings of the algorithm in this article are shown in **Table 8**:

Table 8. RBF neural network algorithm parameters.

Sequence	Parameter	Specifications
1	Learning rate	0.001
2	Number of hidden layers	3
3	Activation function	ReLU
4	Basis function	Gaussian
5	Regularization parameter	0.01
6	Epochs	200
7	Batch size	64
8	Weight initialization	Xavier Initialization
9	Optimizer	Adam

The parameter settings for RF, LSTM, and SVM algorithms are shown in **Table 9**:

Table 9. RF, LSTM, and SVM algorithm parameters.

Sequence	Parameter	Specifications
RF	Number of trees	100
	Maximum depth	10
	Minimum samples split	2
LSTM	Time steps	10
	Number of hidden Units	50
	Learning rate	0.001
SVM	Regularization parameter	1.0
	Kernel function	Sigmoid
	Tolerance	0.1

In parameter selection, for RBF neural networks, the optimal parameter combination is selected through grid search and cross validation methods. The

learning rate is an important parameter that affects the convergence speed and final performance of the model, and it is selected between 0.001 and 0.1 through experiments. To reduce the risk of overfitting, the maximum number of iterations is selected through experimentation between 1000 and 5000, and the optimal number of iterations is chosen between 1000 and 5000. To control the complexity of the model, the optimal regularization parameters are selected between 0.01 and 1.0 through grid search. For RF, the best Number of Trees was selected between 10 and 100 through grid search, and the best Max Depth was selected between 10 and 50. Min Samples Leaf selects between 1 and 10 through experimentation to balance the complexity and generalization ability of the model. For LSTM, the time step determines the length of historical data considered by the model at each time point. The optimal time step was selected between 10 and 50 through experiments, the optimal number of hidden layer elements was selected between 10 and 100 through grid search, and the optimal Learning Rate was selected between 0.001 and 0.1 through experiments. For SVM, select the Sigmoid kernel as the optimal Kernel Function through grid search, including. The Regularization parameter is selected between 0.1 and 10, while the Tolerance parameter is selected between 0.01 and 1.

4.3. Experimental results

(1) Comparison of modeling accuracy

The establishment of a high-precision error model for multi-frequency and multi-system GNSS can not only improve its positioning accuracy, but also enhance its adaptability to various environments and working conditions. This article uses MSE as a measurement index to compare the differences between the error modeling predicted values and actual values of various models. The final result is shown in **Figure 4**:

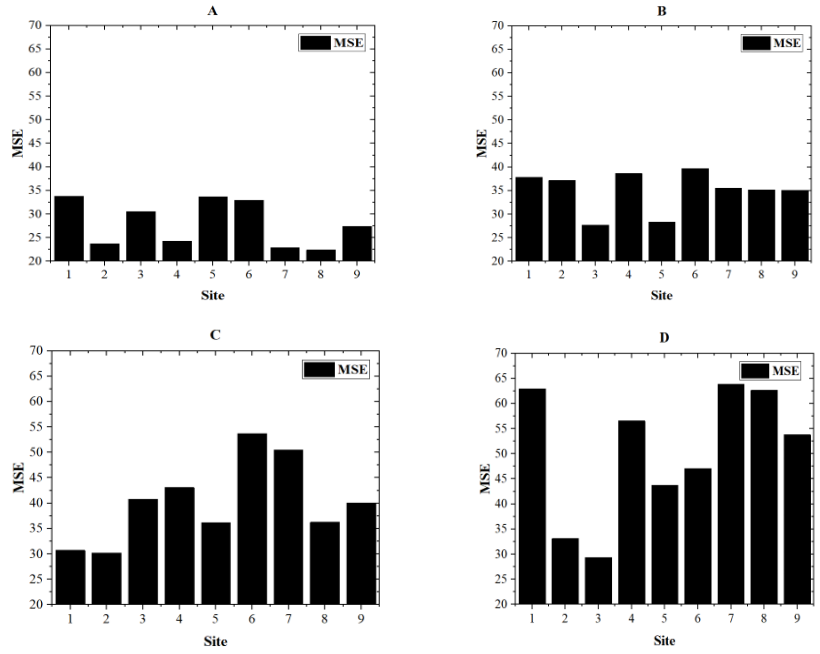

Figure 4. Accuracy comparison results.

Figure 4A shows the accuracy of the RBF neural network;

Figure 4B shows the accuracy of RF;

Figure 4C shows the accuracy of LSTM;

Figure 4D shows the accuracy of SVM.

From **Figure 4**, it can be seen that there are significant differences in the modeling accuracy results of different models at each observation site. In **Figure 4A**, the mean MSE of the model in this article is approximately 27.966; in **Figure 4B**, the mean MSE of RF is approximately 35.013; in **Figure 4C**, the mean MSE of LSTM is approximately 40.152; in **Figure 4D**, the mean MSE of SVM is approximately 50.339; from the specific comparison results, the mean MSE of the RBF neural network in this article decreases by 20.1%, 30.3%, and 44.4% compared to the RF, LSTM, and SVM algorithms, respectively. This result represents that the RBF neural network can more accurately simulate the errors of observation stations.

(2) Improvement degree after correction

On the basis of the modeling accuracy results, the improvement degree of each model before and after multi-frequency and multi-system GNSS positioning error correction is compared. The final result is shown in **Figure 5**:

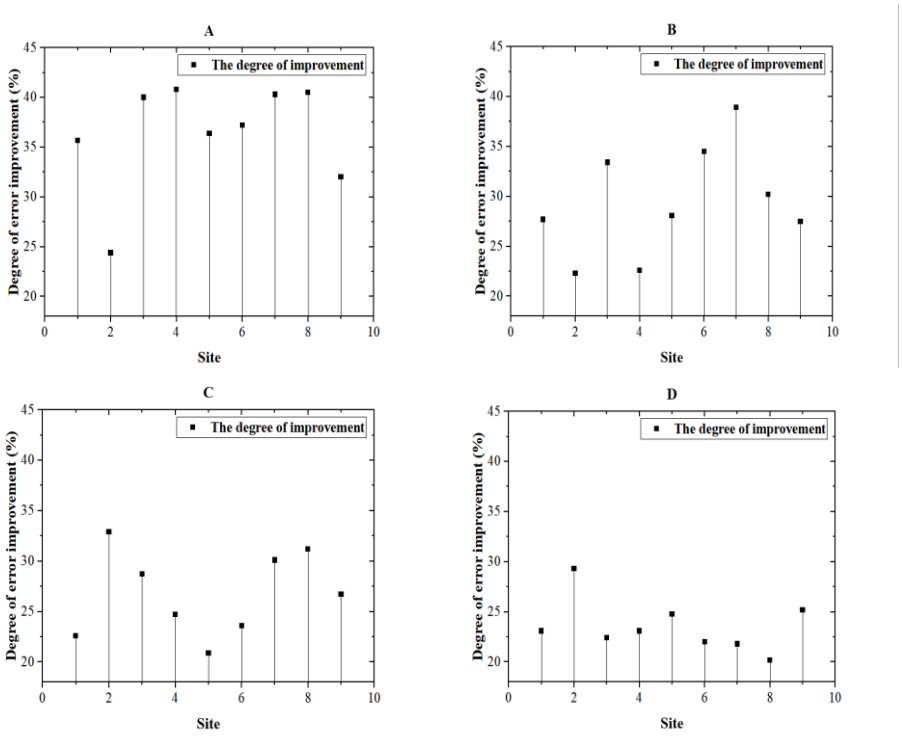

Figure 5. Comparison of improvement after correction.

Figure 5A shows the degree of improvement of RBF neural network;

Figure 5B shows the degree of improvement of RF;

Figure 5C shows the degree of improvement of LSTM;

Figure 5D shows the degree of improvement of SVM.

In the comparison of the improvement degree after calibration in **Figure 5**, it can be seen that based on the error modeling, the improvement degree before and after GNSS positioning error correction using RBF neural network is more significant.

From **Figure 5A**, it can be seen that the average improvement in error after the algorithm model correction in this article is about 36.4%; from **Figure 5B**, the average improvement in error after RF model correction is about 29.5%; from **Figure 5C**, it can be seen that the average improvement in error after LSTM model correction is about 26.8%; from **Figure 5D**, the average improvement in error after SVM model correction is about 23.5%. Compared with the other three types of models, the average improvement level of the model in this article is 6.9%, 9.6%, and 12.9% higher, respectively. This result indicates that using the model proposed in this article for GNSS positioning error correction can improve the overall accuracy and reliability of the positioning system.

(3) Stability

In error modeling and correction, stable models can better adapt to different observation conditions in changing environments, and CV can effectively reflect the discreteness of correction data. The smaller the coefficient of variation, the more consistent the output results of the model. The final CV comparison results of each model are shown in **Figure 6**:

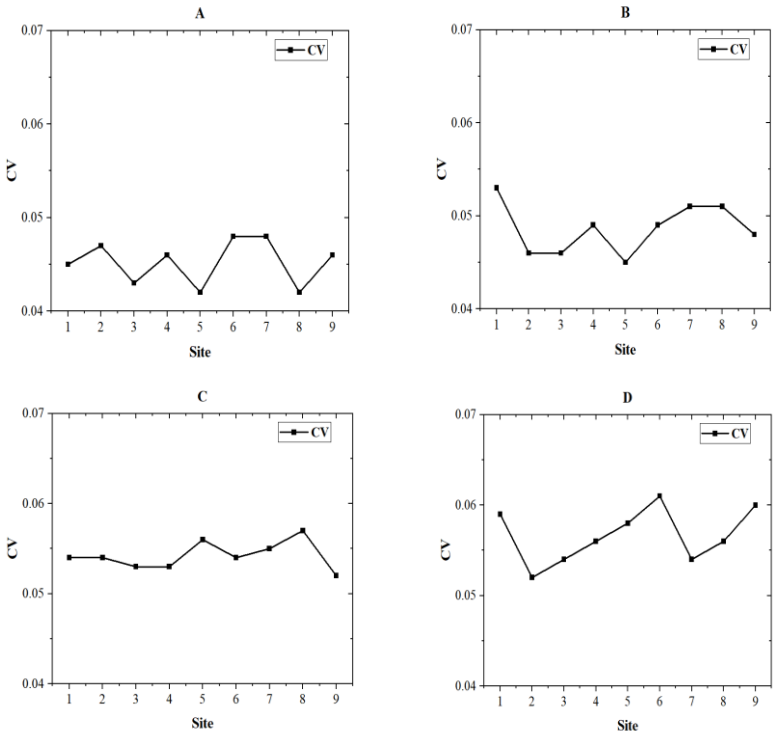

Figure 6. Stability comparison results.

Figure 6A shows the stability of RBF neural network;

Figure 6B shows the stability RF;

Figure 6C shows the stability of LSTM;

Figure 6D shows the stability of SVM.

Figure 6 shows the CV results of calibration data for each model at different sites. In **Figure 6A**, the mean CV of the RBF neural network is 0.045; in **Figure 6B**, the mean CV of the RF model is 0.049; in **Figure 6C**, the mean CV of the LSTM model is 0.054; in **Figure 6D**, the mean CV of the SVM model is 0.057. Compared with RF,

LSTM, and SVM algorithms, the mean CV of RBF neural network correction data decreases by approximately 8.2%, 16.7%, and 21.1%, respectively. This result indicates that the positioning error corrected by the model in this article has lower volatility and better data consistency and stability.

(4) Calculation efficiency

In the face of the increasing demand for fast and accurate positioning services, real-time modeling and correction of GNSS positioning errors are crucial. Efficient models can quickly complete tasks with limited computing resources. This article uses execution time as an indicator to calculate the total time required for each model from input data to model output results, and compares the computational efficiency of different models. The results are shown in **Figure 7**:

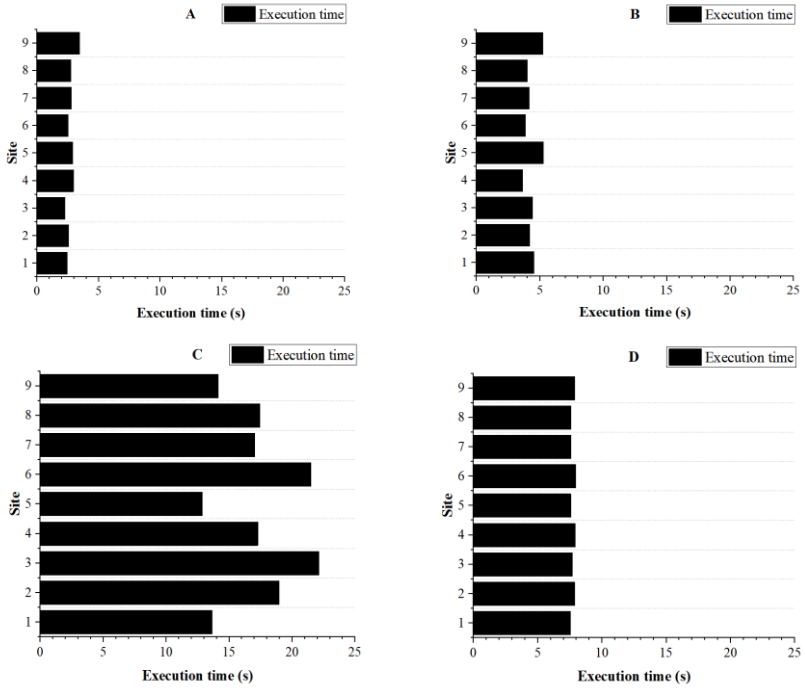

Figure 7. Comparison of computational efficiency results.

Figure 7A shows the computational efficiency of the RBF neural network;

Figure 7B shows the calculation efficiency of RF;

Figure 7C shows the computational efficiency of LSTM;

Figure 7D shows the computational efficiency of SVM.

In **Figure 7**, from the perspective of algorithm execution time, the algorithm proposed in this article generally has higher computational efficiency and lower execution time consumption under different station observation data. In **Figure 7A**, the average execution time of the algorithm in this article is about 2.73 seconds; in **Figure 7B**, the average execution time of the RF algorithm is about 4.37 seconds; in **Figure 7C**, the average execution time of the LSTM algorithm is about 17.22 seconds; in **Figure 7D**, the average execution time of SVM algorithm is about 7.73 seconds. From the comparison of computational efficiency, the average execution time of the algorithm in this article is 37.5%, 84.1%, and 64.7% less than the other three types of models, respectively. The RBF neural network model can process more data under the

same resource conditions, achieving real-time updates of positioning error correction parameters.

5. Discussion

In the experimental analysis, this article verifies the application effect of RBF neural network algorithm in multi-frequency and multi-system GNSS positioning error modeling and correction from four aspects: modeling accuracy, improvement degree after correction, stability, and computational efficiency. In terms of modeling accuracy, compared to the other three types of models, RBF neural networks have higher accuracy results. By using RBF functions as activation functions for hidden neurons, they can effectively approximate complex nonlinear relationships, thereby improving modeling accuracy. From the comparison of the degree of improvement after correction, it can be seen that the model error improvement in this article is more significant. The center point of the model can be automatically adjusted based on training data, enabling the network to better capture key features of the input space and effectively improve errors. From the perspective of stability comparison, the model in this article can maintain good generalization performance between different sites and reduce the fluctuation of prediction results through local response characteristics and center point adaptive adjustment mechanism. From the comparison of computational efficiency, the structure of the model in this article is relatively simple and requires fewer parameters to adjust, which makes the training process faster and consumes less execution time than the other three types of models.

6. Conclusions

This article explores the application of ML algorithm in modeling and correcting positioning errors of multi-frequency and multi-system GNSS. RBF neural network is used for continuous learning and training, and the model is used to achieve modeling and correction of positioning errors. The RBF neural network model has significant advantages in GNSS positioning error correction, which can effectively improve the positioning accuracy of the system while reducing the system's requirements for computing resources, and ensure data consistency and stability. Although this study can provide guidance for improving GNSS positioning services to a certain extent, there are still limitations. This article does not fully consider all possible sources of error in data collection and experimental analysis, and lacks analysis under specific environmental conditions and application scenarios. In future research, it is necessary to consider expanding the sources of errors and combining them with other observational data for multi-source information fusion to improve the reliability and accuracy of the overall positioning system.

Author contributions: Conceptualization, QL and JZ; methodology, QL; software, JZ; validation, YC, JY and SW (Shan Wu); formal analysis, QL; investigation, YC; resources, JZ; data curation, JY; writing—original draft preparation, SW (Sirui Wu); writing—review and editing, SW (Shan Wu); visualization, JZ; supervision, YC; project administration, QL; funding acquisition, JY. All authors have read and agreed to the published version of the manuscript.

Funding: Research and application of transmission line state sensing technology based on Beidou high-precision positioning, supported by science and technology project of Guizhou Electric Power Design and Research Institute Co., LTD., PowerChina, (GZEDKJ-2024-14).

Ethical approval: Not applicable.

Conflict of interest: The authors declare no conflict of interest.

References

1. Jin, Shuanggen, Qisheng Wang, and Gino Dardanelli. "A review on multi-GNSS for earth observation and emerging applications." Remote Sensing 14.16 (2022): 3930-3953. DOI: 10.3390/rs14163930
2. Yasyukevich, Yury V., Baocheng Zhang, and Venkata Ratnam Devanaboyina. "Advances in GNSS Positioning and GNSS Remote Sensing." Sensors 24.4 (2024): 1200-1205. DOI: 10.3390/s24041200
3. Siemuri, Akpojoto, Kannan Selvan, Heidi Kuusniemi, Petri Valisuo, Mohammed S. Elmusrati. "A systematic review of machine learning techniques for GNSS use cases." IEEE Transactions on Aerospace and Electronic Systems 58.6 (2022): 5043-5077. DOI: 10.1109/TAES.2022.3219366
4. Niu, Xiaoji, Yuhang Dai, Tianyi Liu, Qijin Chen, Quan Zhang. "Feature-based GNSS positioning error consistency optimization for GNSS/INS integrated system." Gps Solutions 27.2 (2023): 89-102. DOI: 10.1007/s10291-023-01421-9
5. Sun, Rui, Linxia Fu, Qi Cheng, Kai-Wei Chiang, Wu Chen. "Resilient pseudorange error prediction and correction for GNSS positioning in urban areas." IEEE Internet of Things Journal 10.11 (2023): 9979-9988. DOI: 10.1109/JIOT.2023.3235483
6. Shen, Chong, Yu Zhang, Xiaoting Guo, Xiyuan Chen, Huiliang Cao, Jun Tang, et al. "Seamless GPS/inertial navigation system based on self-learning square-root cubature Kalman filter." IEEE Transactions on Industrial Electronics 68.1 (2020): 499-508. DOI: 10.1109/TIE.2020.2967671
7. Farrell, Jay A., Felipe O. Silva, Farzana Rahman, Jan Wendel. "Inertial measurement unit error modeling tutorial: Inertial navigation system state estimation with real-time sensor calibration." IEEE Control Systems Magazine 42.6 (2022): 40-66. DOI: 10.1109/MCS.2022.3209059
8. Abosekeen, Ashraf, Umar Iqbal, Aboelmagd Noureldin, Michael J. Korenberg. "A novel multi-level integrated navigation system for challenging GNSS environments." IEEE Transactions on Intelligent Transportation Systems 22.8 (2020): 4838-4852. DOI: 10.1109/TITS.2020.2980307
9. Morales, Joshua J., and Zaher M. Kassas. "Tightly coupled inertial navigation system with signals of opportunity aiding." IEEE Transactions on Aerospace and Electronic Systems 57.3 (2021): 1930-1948. DOI: 10.1109/TAES.2021.3054067
10. Li, Zhen, Lu Tieding, Yu Kegen, Wang Jie. "Interpolation of GNSS Position Time Series Using GBDT, XGBoost, and RF Machine Learning Algorithms and Models Error Analysis." Remote Sensing 15.18 (2023): 4374-4392. DOI:10.3390/rs15184374
11. Chen, Jianping, and Yang Gao. "A Machine Learning-Based Tropospheric Prediction Approach for High-Precision Real-Time GNSS Positioning." Sensors 24.10 (2024): 2957-2972. DOI: 10.3390/s24102957
12. Li, Changle, Yuchuan Fu, Fei Richard Yu, Tom H. Luan, Yao Zhang. "Vehicle position correction: A vehicular blockchain networks-based GPS error sharing framework." IEEE Transactions on Intelligent Transportation Systems 22.2 (2020): 898-912. DOI: 10.1109/TITS.2019.2961400
13. Fang, Wei, Jiang Jinguang, Lu Shuangqiu, Gong Yilin, Tao Yifeng, Peihui Yan, et al. "A LSTM algorithm estimating pseudo measurements for aiding INS during GNSS signal outages." Remote sensing 12.2 (2020): 256-279. DOI:10.3390/rs12020256
14. Ramavath, Anil Kumar, and Naveen Kumar Perumalla. "A machine-learning approach to estimate satellite-based position errors." Journal of Applied Geodesy 18.2 (2024): 335-344. DOI: 10.1515/jag-2023-0051
15. Chen, Jian, Xingwang Zhao,Chao Liu,Shaolin Zhu,Zhiqiang Liu and Dongjie Yue. "Evaluating the latest performance of precise point positioning in multi-GNSS/RNSS: GPS, GLONASS, BDS, Galileo and QZSS." The journal of navigation 74.1 (2021): 247-267. DOI: 10.1017/S0373463320000508

16. Lou, Yidong, Dai Xiaolei, Gong Xiaopeng, Li Chenglong, Qing Yun, Liu Yang, et al. “A review of real-time multi-GNSS precise orbit determination based on the filter method.” Satellite navigation 3.1 (2022): 1-15. DOI: 10.1186/s43020-022-00075-1
17. Rodriguez-Alvarez, Nereida, Joan Francesc Munoz-Martin, and Mary Morris. “Latest advances in the global navigation satellite system—reflectometry (GNSS-R) field.” Remote Sensing 15.8 (2023): 2157-2185. DOI:10.3390/rs15082157
18. Shen, Nan, Chen Liang, Wang Lei, Chen Ruizhi. “GNSS Site unmodeled error prediction based on machine learning.” GPS Solutions 27.2 (2023): 77-92. DOI: 10.1007/s10291-023-01411-x
19. Panda, Sashmita, and Ganapati Panda. “On the development and performance evaluation of improved radial basis function neural networks.” IEEE Transactions on Systems, Man, and Cybernetics: Systems 52.6 (2021): 3873-3884. DOI: 10.1109/TSMC.2021.3076747
20. Shaukat, Nabil, Ahmed Ali, Muhammad Javed Iqbal, Muhammad Moinuddin and Pablo Otero. “Multi-sensor fusion for underwater vehicle localization by augmentation of rbf neural network and error-state kalman filter.” Sensors 21.4 (2021): 1149-1174. DOI:10.3390/s21041149